

# Higher-Order Topological States in Photonic Thue-Morse Quasicrystals: Quadrupole Insulator and the Origin of Corner States

Langlang Xiong,<sup>1,3</sup> Yu Zhang,<sup>2,3</sup> Yufu Liu,<sup>2,3</sup> Yaoxian Zheng,<sup>4</sup> and Xunya Jiang<sup>1,2,3,\*</sup>

<sup>1</sup>*Institute of Future Lighting, Academy for Engineering and Technology, Fudan University, Shanghai 200433, China*

<sup>2</sup>*Department of Illuminating Engineering and Light Sources, School of Information Science and Engineering, Fudan University, Shanghai 200433, China*

<sup>3</sup>*Engineering Research Center of Advanced Lighting Technology, Fudan University, Ministry of Education, Shanghai 200433, China*

<sup>4</sup>*THz Technical Research Center and College of Physics and Optoelectronic Engineering, Shenzhen University, Shenzhen 518060, China*

(Received 25 July 2022; revised 19 October 2022; accepted 22 November 2022; published 29 December 2022)

Corner states (CSs) in higher-order topological insulators (HOTIs) have recently been of great interest in both crystals and quasicrystals. In contrast to electronic systems, HOTIs have not been found in photonic quasicrystals (PQCs). Here, we systematically study the higher-order topology in the two-dimensional Thue-Morse photonic quasicrystals (TM PQCs). Not only the topological phase transition and the nontrivial CSs with fractional charge induced by multipole moments, but also another type of CSs are found due to the complex structure of TM PQCs near corners. The different origins of these CSs are also analyzed based on the tight-binding model. Our work opens the door to explore richer HOT physics beyond photonic crystals and the robustness of CSs in PQC shows the potential for applications.

DOI: 10.1103/PhysRevApplied.18.064089

## I. INTRODUCTION

In the research of topological systems [1–11], higher-order topology (HOT) has become a hot spot since it could lead to unique topological states beyond traditional bulk-boundary correspondence [12–18]. Specifically, kinds of two-dimensional (2D) higher-order topological insulators (HOTIs), i.e., quadrupole insulators (QIs) [19–21], whose topological invariant, quadrupole moments  $q_{xy}$ , is quantized to 0 or 0.5 if the system presents fourfold rotation symmetry  $C_4$  or mirror symmetries  $M_x := x \rightarrow -x$  and  $M_y := y \rightarrow -y$ , and nonzero  $q_{xy}$  can give rise to the zero-dimensional (0D) nontrivial corner states (CSs), namely type-I CSs. Besides, additional type-II CSs that are caused by long-range interactions have also been found [22–24].

Very recently, the concept of HOTIs has extended from periodic crystals to quasicrystals (QCs) and aperiodic crystals [25–32], which also show nontrivial zero-energy CSs in the 2D quantum system. However, in contrast to the study of HOTIs in electronic systems based on the tight-binding model (TBM), the realizations and physical properties of HOTIs in photonic quasicrystals (PQCs) have not been studied, which have abundant applications in reality.

Even more, the research for HOT CSs of the electronic systems concentrates on type-I CSs, so we still cannot answer such questions, such as “in QCs, can we realize richer CSs, or even find different origins of CSs beyond the two types of CSs in crystals?”

In this work, we systematically investigate the HOT properties of 2D Thue-Morse (TM) PQCs [33,34]. We first construct a TM PQC with two kinds of dielectric rods, then a TBM base on the TM PQC is built. By tuning difference parameters of TBM, the HOT phase transition with nonzero  $q_{xy}$  is found. Moreover, the different origins of CSs in PQCs are revealed by using the weak-coupling limit [18,22,35]. From the different origins, we demonstrate that, besides the type-I CSs with fractional charges and the type-II CSs from long-range interactions, there is another type of CS from the complex structure of TM PQCs, which is independent of long-range interactions and beyond the periodic systems. Finally, based on the strict numerical simulation, we show that all these CSs can exist in real TM PQCs and CSs from TM PQCs could be more robust compared with those in photonic crystals (PhCs). This work is valuable in expanding the understanding of HOT phases beyond periodic photonic systems and observing CSs in PQCs with special properties, which can be further utilized to design the aimed devices with topological protection.

\*jiangxunya@fudan.edu.cn

## II. MODEL AND TOPOLOGICAL PHASE TRANSITION

A 2D TM sequence  $S_N$  of order  $N$  can be deduced by

$$S_N = \begin{bmatrix} S_{N-1} & \tilde{S}_{N-1} \\ \tilde{S}_{N-1} & S_{N-1} \end{bmatrix} \quad \text{and} \quad S_1 = \begin{bmatrix} A & B \\ B & A \end{bmatrix}, \quad (1)$$

where  $\tilde{S}_{N-1}$  is obtained by exchanging  $A$  and  $B$  in  $S_{N-1}$ . The photonic model of 2D square TM sequence can be generated by placing different dielectric rods in the square lattice. In particular, TM photonic structure of basic sequences  $S_1$  and  $\tilde{S}_1$  is shown in Fig. 1(a), and we mark them with basic square cells. The four corners of a square cell contain four dielectric rods in the air with radius  $r = 0.12a$ , where  $a$  is the side length of a square cell. The dielectric rods are divided into two types: rods  $A$  with relative permittivities  $\epsilon_A$  and relative permeability  $\mu_A$ , and rods  $B$  with  $\epsilon_B$  and  $\mu_B$ . Then, we can use Eq. (1) and square cell  $S_1$  to deduce higher-order TM PQC, e.g., Fig. 1(a) shows a PQC of  $S_4$  TM sequence. We can find a TM PQC of even order has  $C_4$  and  $M_{x(y)}$  symmetries, whereas TM PQC of odd order does not.

In recent works [16,18,22], it is found that TBM is a good platform to reveal the origins of topological states in the photonic systems for the lower bands. Following this path, we also construct a TBM base on TM PQC, which is shown in Fig. 1(b). The on-site energy of rods  $A(B)$  is  $U_{A(B)}$ . Considering the frequency difference of Mie resonances of two kinds of rods, the nearest-neighbor coupling between rod  $A$  and rod  $B$   $t_1$  is supposed to be a small value generally. The intercell coupling between two rods  $A$  (or  $B$ ) is  $t_{2(3)}$ , and the next-nearest-neighbor (NNN) coupling between two rods  $A$  (or  $B$ ) of the intercell on the diagonal direction is  $t_{4(5)}$ , which can open the gap at energy  $E = 0$ . In Fig. 1(c), for the convenience of our further study, TBM of the limiting case with  $t_1 = 0$  is shown, in which the

entire structure splits into three types of isolated clusters: two tetramers, four dimers, and two singles. The dimers in diagonal directions and in horizontal (vertical) directions are marked with dimers I and dimers II, respectively. Such a split model is helpful for us to analyze the origins of different topological states in the next section. Note that the coupling between the same type of rod inside one cell is neglected due to the large distance between them and we emphasize this by a red cross in the top left corner in Fig. 1(c).

To focus on the process of topological phase transition, we introduce a variable  $t_0$  and set  $t_1 = 1 - t_0$ ,  $t_2 = t_3 = 1 + t_0$ ,  $t_4 = -t_5 = 3.5t_2$ , and  $U_A = U_B = 0$ . In Fig. 2(a), the band structure of open boundary condition versus  $t_0 \in [-1, 1]$  are drawn. By using real space method [20,36–40], we calculate the quadrupole moment  $q_{xy}$  of the gap at  $E = 0$  versus different  $t_0$  in Fig. 2(b). We can see  $q_{xy}$  jumps from 0 to 0.5 for  $t_0$  from  $-1$  to  $1$ , which means a topological phase transition, and the main jumping happens near  $t_0 = 0$ , i.e.,  $t_1 = t_2 = t_3$ . Specifically, we choose  $t_0 = 0.6$  and its band structure is shown in Fig. 2(c), where type-I CSs at zero energy that are protected by nonzero quadrupole moment are marked with red dots. The topological nontriviality of CSs is also confirmed by the index requirement from the filling anomaly theory [20] that the indices of CSs in our model are 127–130. Figure 2(e)–D shows a typical distribution of type-I CS. What is more, we calculate the sum of the lowest half states to show direct distributions of fractional corner charges [40], which can be proved to be equal to quadrupole moment [19]. In Fig. 2(f), we set a large  $t_0 = 0.999$  to obtain more localized CSs, and the distributions of corner charges that are calculated by the local density of states (LDOS) are shown. It is found that the fractional corner charge is quantized to 0.5, which is because of  $C_4$  and  $M_{x(y)}$  symmetries, and the edge charge remains zero because of  $C_2$  symmetry [20]. It should be noted that the labels of  $x(a)$  and  $y(a)$  that go

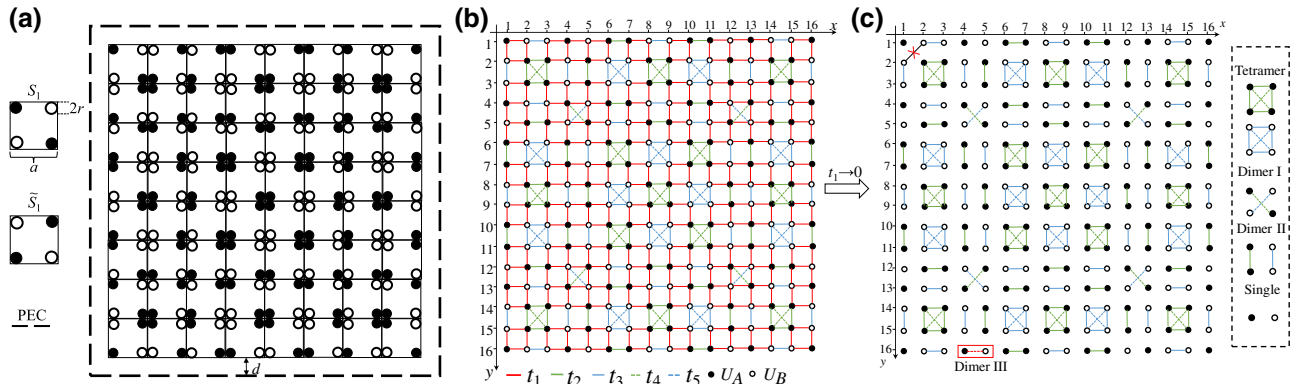


FIG. 1. (a) The  $S_4$  TM PQCs with rods  $A$  and rods  $B$ , the PEC boundary is marked with black dash lines; (b) the TBM bases on the 2D TM PQC; (c) the limiting case of TBM with  $t_1 = 0$ .

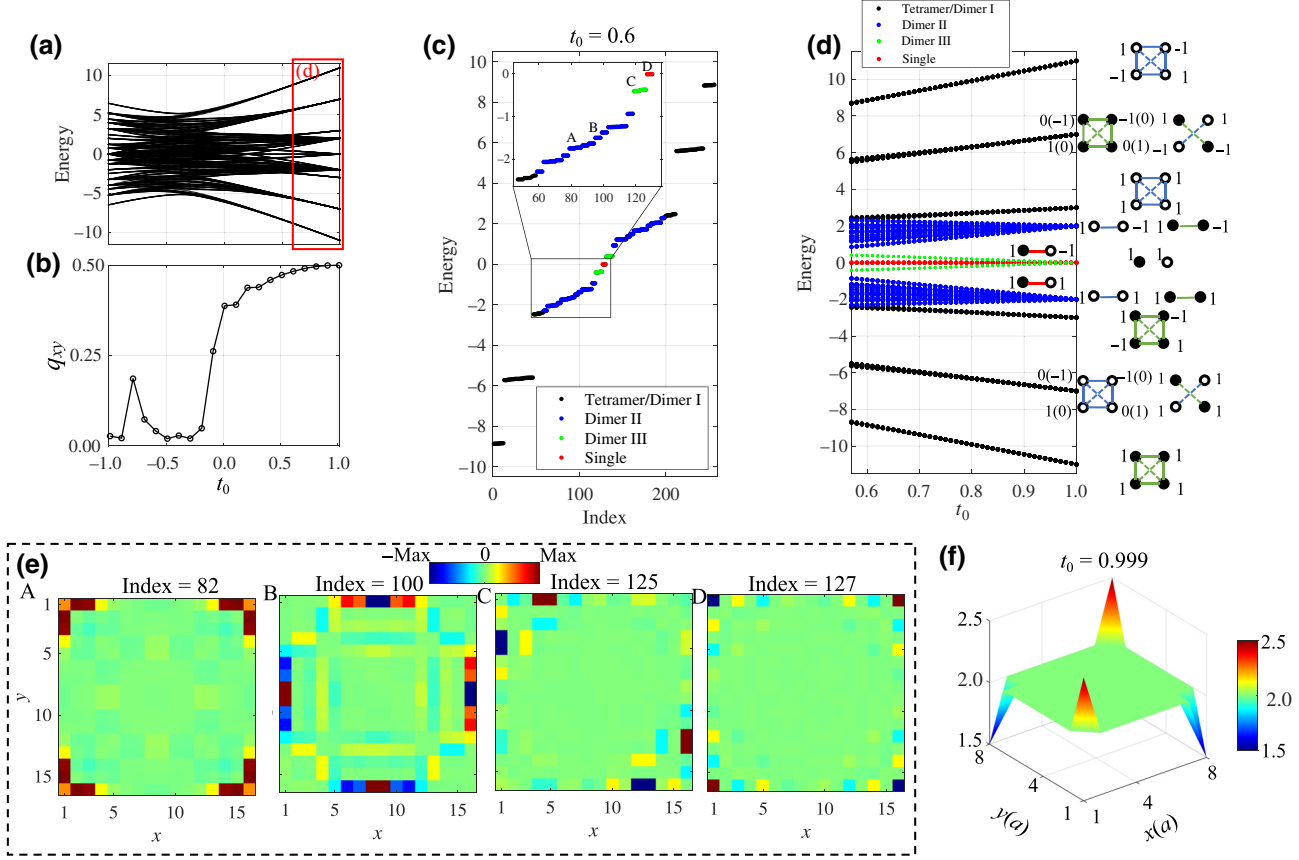


FIG. 2. (a) The band structure of  $S_4$  TM QC with open boundary condition versus  $t_0 \in [-1, 1]$ , other parameters are set as  $t_1 = 1 - t_0$ ,  $t_2 = t_3 = 1 + t_0$ ,  $t_4 = -t_5 = 3.5t_2$ , and  $U_A = U_B = 0$ ; (b) the quadrupole moment  $q_{xy}$  versus different  $t_0$ ; (c) the band structure of  $S_4$  TM QC with  $t_0 = 0.6$ , four typical localized states are marked with A–D; (d) the local enlarged (a) for the topological nontrivial region; (e) four localized states that are marked in (c); (f) the distributions of LDOS with  $t_0 = 0.999$ .

from 1 to 8 only, instead of 1 to 16 (see section S1 within the Supplemental Material [40]).

### III. THE ORIGINS OF CSS IN TM QC

Besides type-I CSs that are protected by quadrupole moment, some other localized states in TM QC can also be observed. For example, we choose four typical localized states that are marked in Fig. 2(c) as A–D, and the four states are drawn in Fig. 2(e). In addition to nontrivial type-I CS has been mentioned in Fig. 2(e)-D, there are two CSs in Fig. 2(e)-A and (e)-C and one edge state (ES) in Fig. 2(e)-B. The two CSs in Fig. 2(e)-A and (e)-C are not very localized as type-I CSs and are more likely to be recognized as the type-II CSs [18,22]. However, in our model the NNN coupling between the same rods in one cell is neglected, which is essential for the existence of type-II CSs, so the physical origin of CSs in Fig. 2(e)-A and (e)-C should be reconsidered carefully.

First, we need to go back to Fig. 1(c) in the limiting case  $t_1 = 0$  to reveal the different origins of such types of CSs in Figs. 2(e)-A and (e)-C. According to Fig. 1(c), we

can obtain some basic clues of the state origin from the local split structures. Second, we can analyze the origin of states in Fig. 2 more carefully. Specifically, we enlarge the area of the red rectangle in Fig. 2(a) and show the area in Fig. 2(d), where  $t_1 = 1 - t_0$  is a small value compared with other coupling terms since  $t_0 > 0.6$ . In Fig. 2(d), we mark the states with different colors according to their different cluster origins, e.g., the states from tetramers and dimers I, dimers II, dimers III, and singles are marked with black, blue, green, and red dots, respectively. On the right side of Fig. 2(d) near every band, in the limit  $t_0 = 1$  ( $t_1 = 0$ ), we also show the symmetry property of the states for different clusters. Next, we introduce more details of these states from different clusters, which could be solved theoretically. First, the tetramers support six eigenstates, two singlet quadrupole modes with  $E = -t_{4(5)} + 2t_{2(3)}$ , two doublets of dipolar modes with  $E = t_{4(5)}$ , and two singlet monopolar modes with  $E = -t_{4(5)} - 2t_{2(3)}$ . Second, dimers I and dimers II support eight dipolar modes: symmetric modes with  $E = -t_{2,3,4,5}$  and antisymmetric modes with  $E = t_{2,3,4,5}$ . Third, the singles support two eigenstates with  $E = 0$  since  $U_A = U_B = 0$ .

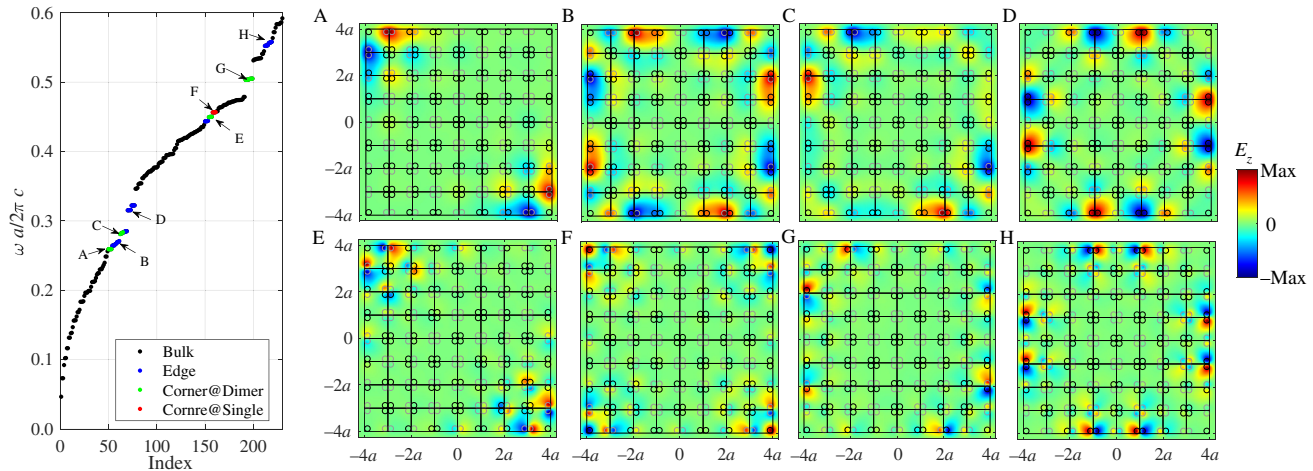


FIG. 3. Band structure of a  $S_4$  TM PQC with  $\varepsilon_A = 10$ ,  $\varepsilon_B = 16$ , and PEC boundary. The distance between PEC and PQC is  $d = 0.25a$ . Eight typical states are marked with A–H, and the  $E_z$  field distributions of those states are also shown on the right, where black (gray) circles are rods A(B).

If we introduce nonzero but small  $t_1$ , we can find topological phenomena in our 2D TM systems, like or unlike 2D crystals. For example, when we set  $t_0 = 0.6$ , the ESs shown in Fig. 2(e)-B and the type-I CSs shown in Fig. 2(e)-D could be observed, similar to the crystals. From the field distribution and the energy, we find that the ESs are from dimers II structure and located at the system edges. For the type-I CSs, we find they are from singles at the corners of the system. So the origin of these ESs and CSs are similar to crystals. However, since the structure of 2D TM systems are much more complex than 2D crystals, some states could be observed in the gaps, like the states shown in Figs. 2(e)-A and 2(e)-C, which need to be carefully investigated and are beyond 2D crystals.

For the state in Fig. 2(e)-A, we need go back to Fig. 1(c). From the field distribution of the state and the structure on the corner in Fig. 1(c), we can see that the state originated from the coupling of two dimers II near the corners by the corner single. We note that this type of CS is different from the type-II CSs in crystals [18,22] since we suppose no NNN coupling in our model. For the state in Fig. 2(e)-A whose energy is shown by the green points in Fig. 2(d), its origin is quite counterintuitive since when  $t_0 = 1$  its energy will converge to zero, the energy of singles. As we have shown in Fig. 1(c), there are two singles (e.g.,  $A$ -kind rod at position 4 and  $B$ -kind rod at position 5 at both edges) near the corner, which is because of the complex structure of 2D TM systems. Since the coupling  $t_1 = 1 - t_0$  between two kinds of rods is not zero now, these two singles can couple to each other and form a kind of dimer, which is named dimers III. From the field distribution in Fig. 2(e)-C, we can see that this type of CS is from the coupling between two dimers III near the corner. Hence, when  $t_0 \rightarrow 1$  ( $t_1 \rightarrow 0$ ), the energy of the CS converges to zero since these coupled singles are almost decoupled from

each other. Obviously, the origin of those two types of CSs are from the complex 2D TM structure, and we mark them as CSs from structures.

*Photonic HOTIs.*—In this section, we study the real photonic TM systems to show that all those HOT states can be realized in real PQCs by strict numerical results from the software without any approximation, i.e., finite-element method (FEM) software COMSOL Multiphysics. Furthermore, from the analyses with defects or randomness, it is found that the CSs in PQCs could be more robust than the type-II CSs in PhCs. Here, we hope to note that, according to the analysis based on TBM, the coupling terms correspond to the couplings between the rods, not the on-site energies correspond to the Mie resonant frequencies of rods, which are the dominant reason for the existence of HOTIs. Hence, in real PQCs, rods  $A$  and rods  $B$  are set to be with different permittivities but the same radius to ensure the relative strengths of couplings between the rods are similar to coupling terms of TBM, but with the side effect of the different frequencies of Mie resonances [41].

Now, we consider a 2D TM PQC with  $\varepsilon_A = 10$ ,  $\varepsilon_B = 16$ ,  $\mu_A = \mu_B = 1$ ,  $N = 4$ , and the perfect electrical conductor (PEC) boundary is used, where the distance between PEC and PQC is  $d = 0.25a$ . In Fig. 3, the eigenstates of  $E_z$  polarization are shown, in which bulk states, edge states, and corner states at dimers or singles are marked with black, blue, green, and red dots, respectively. We select eight typical states from low frequency to high frequency, which are marked with A–H, and  $E_z$  field distributions of those states are also shown, where black (gray) circles are rods A(B). It is easy to find the ESs in Fig. 3-B, -D, and -H. Furthermore, there are three types of CSs in the TM PQC: nontrivial CS at single rods is shown in Fig. 3-F, CSs at dimers II are shown in Fig. 3-A and -E, and CSs at

dimers III are shown in Fig. 3-C and -G, and the counterparts of those three types of CSs in TBM can be found in Fig. 2(e)-D, -A, and -C, respectively. The symmetric features of CSs at dimers are also the same as the results of TBM, i.e., CSs of lower frequencies are symmetric along the center of dimers, while CSs of higher frequencies are antisymmetric.

What is more, we can calculate the topological invariant of PQCs, which form bulk states by using the real space method [40]. In particular, the dipole moments  $p_i^n$  (where  $n$  is the  $n$ th gap and  $i$  is direction) for the PQC of the first and second gap are  $p_x^1 = p_y^1 = 0.5$  and  $p_x^2 = p_y^2 = 0$ , respectively, and the quadrupole moments of the second gap are near  $q_{xy} = 0.5$ . Proving that the nontrivial type-I CSs at the first gap are induced by dipole moments [16], while at the second gap are induced by quadrupole moments [18,20] (see section S2 within the Supplemental Material [40]). Surprisingly, the solution numbers of type-I CSs of PQCs do not satisfy the filling anomaly theory for traditional type-I CSs of PhCs. The violation may be from the much more complex photonic band-gap structure of TM PQC and we will investigate it in further work.

It should be emphasized that CSs from structures are independent of NNN coupling, so these types of CSs found in this work could be more robust than type-II CSs in PhCs, which is a useful property for real applications. For example, in section S3 within the Supplemental Material [40], we use a small defect to reduce the influence of NNN coupling, e.g., change the radius of rods near the corner, and we find the CSs in the TM PQC still exist, but type-II CSs in PhC disappear. Moreover, the presence of dislocations of rods in TM PQC is also considered to simulate the real materials with imperfections, that is, we change the positions of the rods near the concerned corner of TM PQC, and all types of CSs that are localized at the concerned corner are almost unchanged, so the robustness of the CSs in the TM PQCs is demonstrated.

In addition to the results of  $S_4$  TM sequence, the results of  $S_6$  TM sequence are also shown in section S5 within the Supplemental Material, where CSs are similar to those of  $S_4$  TM sequence, except that CSs from dimers are more localized at the corners and easier to be observed.

#### IV. CONCLUSION

In summary, we demonstrate that the topological nontrivial CSs from multipole moments, can be realized in PQCs, whose structure is without translational symmetry. What is more, the types of CSs are found since the complex structure of PQCs near the corners, so the CSs from structures could be very universal in other QCs [42], even in a QC without both rotation and mirror symmetries, such as Fibonacci PQCs [43] (see section S7 within the Supplemental Material). Our results reveal rich topological physics in PQCs. The CSs extend our

understanding of HOT phases and can be used to design devices since the all-dielectric structure of PQCs. We also believe CSs widely exist for other waves, e.g., in electronic and phononic QCs, and the research on these topics could be attractive.

#### ACKNOWLEDGMENTS

This work is supported by National High Technology Research and Development Program of China (17-H863-04-ZT-001-035-01); National Key Research and Development Program of China (2016YFA0301103, 2018YFA0306201); National Natural Science Foundation of China (12174073). We thank the topology course team for their open-source codes about the real-space method [38].

- [1] X.-L. Qi and S.-C. Zhang, Topological insulators and superconductors, *Rev. Mod. Phys.* **83**, 1057 (2011).
- [2] M. Z. Hasan and C. L. Kane, Colloquium: Topological insulators, *Rev. Mod. Phys.* **82**, 3045 (2010).
- [3] A. Bansil, H. Lin, and T. Das, Colloquium: Topological band theory, *Rev. Mod. Phys.* **88**, 021004 (2016).
- [4] C.-K. Chiu, J. C. Y. Teo, A. P. Schnyder, and S. Ryu, Classification of topological quantum matter with symmetries, *Rev. Mod. Phys.* **88**, 035005 (2016).
- [5] T. Ozawa, H. M. Price, A. Amo, N. Goldman, M. Hafezi, L. Lu, M. C. Rechtsman, D. Schuster, J. Simon, O. Zilbermanberg, and I. Carusotto, Topological photonics, *Rev. Mod. Phys.* **91**, 015006 (2019).
- [6] M. S. Rider, S. J. Palmer, S. R. Pocock, X. Xiao, P. Arroyo Huidobro, and V. Giannini, A perspective on topological nanophotonics: Current status and future challenges, *J. Appl. Phys.* **125**, 120901 (2019).
- [7] L. Lu, J. D. Joannopoulos, and M. Soljačić, Topological photonics, *Nat. Photonics* **8**, 821 (2014).
- [8] A. B. Khanikaev and G. Shvets, Two-dimensional topological photonics, *Nat. Photonics* **11**, 763 (2017).
- [9] Y. Wu, C. Li, X. Hu, Y. Ao, Y. Zhao, and Q. Gong, Applications of topological photonics in integrated photonic devices, *Adv. Opt. Mater.* **5**, 1700357 (2017).
- [10] G. Hu, Q. Ou, G. Si, Y. Wu, J. Wu, Z. Dai, A. Krasnok, Y. Mazor, Q. Zhang, Q. Bao, Cheng-Wei Qiu, and Andrea Alù, Topological polaritons and photonic magic angles in twisted  $\alpha$ -MoO<sub>3</sub> bilayers, *Nature* **582**, 209 (2020).
- [11] L. Xiong, Y. Zhang, and X. Jiang, Resonance and topological singularity near and beyond zero frequency for waves: Model, theory, and effects, *Photon. Res.* **9**, 2024 (2021).
- [12] G. van Miert and C. Ortix, On the topological immunity of corner states in two-dimensional crystalline insulators, *Npj Quantum Mater.* **5**, 1 (2020).
- [13] M. Kim, Z. Jacob, and J. Rho, Recent advances in 2D, 3D and higher-order topological photonics, *Light: Sci. Appl.* **9**, 1 (2020).
- [14] B. Xie, H.-X. Wang, X. Zhang, P. Zhan, J.-H. Jiang, M. Lu, and Y. Chen, Higher-order band topology, *Nat. Rev. Phys.*, **3**, 520 (2021).

- [15] Y. Liu, S. Leung, F.-F. Li, Z.-K. Lin, X. Tao, Y. Poo, and J.-H. Jiang, Bulk–disclination correspondence in topological crystalline insulators, *Nature* **589**, 381 (2021).
- [16] B.-Y. Xie, H.-F. Wang, H.-X. Wang, X.-Y. Zhu, J.-H. Jiang, M.-H. Lu, and Y.-F. Chen, Second-order photonic topological insulator with corner states, *Phys. Rev. B* **98**, 205147 (2018).
- [17] B.-Y. Xie, G.-X. Su, H.-F. Wang, H. Su, X.-P. Shen, P. Zhan, M.-H. Lu, Z.-L. Wang, and Y.-F. Chen, Visualization of Higher-Order Topological Insulating Phases in Two-Dimensional Dielectric Photonic Crystals, *Phys. Rev. Lett.* **122**, 233903 (2019).
- [18] L. Xiong, Y. Liu, Y. Zhang, Y. Zheng, and X. Jiang, Topological properties of a two-dimensional photonic square lattice without  $C_4$  and  $M_{x(y)}$  symmetries, *ACS Photonics* **9**, 2448 (2022).
- [19] W. A. Benalcazar, B. A. Bernevig, and T. L. Hughes, Quantized electric multipole insulators, *Science* **357**, 61 (2017).
- [20] L. He, Z. Addison, E. J. Mele, and B. Zhen, Quadrupole topological photonic crystals, *Nat. Commun.* **11**, 1 (2020).
- [21] W. A. Benalcazar, B. A. Bernevig, and T. L. Hughes, Electric multipole moments, topological multipole moment pumping, and chiral hinge states in crystalline insulators, *Phys. Rev. B* **96**, 245115 (2017).
- [22] M. Li, D. Zhirihin, M. Gorlach, X. Ni, D. Filonov, A. Slobozhanyuk, A. Alù, and A. B. Khanikaev, Higher-order topological states in photonic kagome crystals with long-range interactions, *Nat. Photonics* **14**, 89 (2020).
- [23] S. lei Shen, C. Li, and J.-F. Wu, Investigation of corner states in second-order photonic topological insulator, *Opt. Express* **29**, 24045 (2021).
- [24] X.-W. Xu, Y.-Z. Li, Z.-F. Liu, and A.-X. Chen, General bounded corner states in the two-dimensional Su-Schrieffer-Heeger model with intracellular next-nearest-neighbor hopping, *Phys. Rev. A* **101**, 063839 (2020).
- [25] R. Chen, C.-Z. Chen, J.-H. Gao, B. Zhou, and D.-H. Xu, Higher-Order Topological Insulators in Quasicrystals, *Phys. Rev. Lett.* **124**, 036803 (2020).
- [26] B. Lv, R. Chen, R. Li, C. Guan, B. Zhou, G. Dong, C. Zhao, Y. Li, Y. Wang, H. Tao, Jinhui Shi, and Dong-Hui Xu, Realization of quasicrystalline quadrupole topological insulators in electrical circuits, *Commun. Phys.* **4**, 1 (2021).
- [27] Y.-S. Hu, Y.-R. Ding, J. Zhang, Z.-Q. Zhang, and C.-Z. Chen, Disorder and phase diagrams of higher-order topological insulators, *Phys. Rev. B* **104**, 094201 (2021).
- [28] J.-H. Wang, Y.-B. Yang, N. Dai, and Y. Xu, Structural-Disorder-Induced Second-Order Topological Insulators in Three Dimensions, *Phys. Rev. Lett.* **126**, 206404 (2021).
- [29] H. Huang, J. Fan, D. Li, and F. Liu, Generic orbital design of higher-order topological quasicrystalline insulators with odd five-fold rotation symmetry, *Nano Lett.* **21**, 7056 (2021).
- [30] T. Biesenthal, L. J. Maczewsky, Z. Yang, M. Kremer, M. Segev, A. Szameit, and M. Heinrich, Fractal photonic topological insulators, *Science* **376**, 1114 (2022).
- [31] B. Yan, J. Xie, E. Liu, Y. Peng, R. Ge, J. Liu, and S. Wen, Topological Edge State in the Two-Dimensional Stampfli-Triangle Photonic Crystals, *Phys. Rev. Appl.* **12**, 044004 (2019).
- [32] Y. Peng, E. Liu, B. Yan, J. Xie, A. Shi, P. Peng, H. Li, and J. Liu, Higher-order topological states in two-dimensional Stampfli-Triangle photonic crystals, *Opt. Lett.* **47**, 3011 (2022).
- [33] Y. Zhang, L. Xiong, M. Zhang, and X. Jiang, Fractal topological band-gap structure induced by singularities in the one-dimensional Thue-Morse system, *Photon. Res.* **9**, 622 (2021).
- [34] L. Moretti and V. Mocella, Two-dimensional photonic aperiodic crystals based on Thue-Morse sequence, *Opt. Express* **15**, 15314 (2007).
- [35] F. Liu and K. Wakabayashi, Novel Topological Phase with a Zero Berry Curvature, *Phys. Rev. Lett.* **118**, 076803 (2017).
- [36] R. Resta, Quantum-Mechanical Position Operator in Extended Systems, *Phys. Rev. Lett.* **80**, 1800 (1998).
- [37] W. A. Wheeler, L. K. Wagner, and T. L. Hughes, Many-body electric multipole operators in extended systems, *Phys. Rev. B* **100**, 245135 (2019).
- [38] Topology course team, Different approaches to topological invariants, <https://topocondmat.org/w8/general/invariants.html> (2021).
- [39] B. Kang, K. Shiozaki, and G. Y. Cho, Many-body order parameters for multipoles in solids, *Phys. Rev. B* **100**, 245134 (2019).
- [40] See Supplemental Material at <http://link.aps.org-supplemental/10.1103/PhysRevApplied.18.064089> for the calculative methods of the topological invariant and local density of states, and discussions of robustness, higher-order TMPQCs, Fibonacci PQC, and tight-binding Hamiltonian.
- [41] The Mie resonant frequencies of one rod in real PQC can analogy with the on-site energies of one site in tight-binding model, and the coupling strength between different rods in real PQC can analogy with the coupling terms in tight-binding model. If the permittivities of rods in PQC are changed, the Mie resonant frequency and coupling also will be changed. From the analyses of tight-binding model, we can find that the relative magnitudes of hopping terms are dominant for the existing of different HOTI. Hence, we can change the permittivities of rods to turn the coupling strength, and influences of the changes of on-site energies can be almost neglected.
- [42] A. Shi, J. Jiang, Y. Peng, P. Peng, J. Chen, and J. Liu, Multimer analysis method reveals higher-order topology in quasicrystals, arXiv preprint [arXiv:2209.05751](https://arxiv.org/abs/2209.05751) (2022).
- [43] A. Poddubny and E. Ivchenko, Photonic quasicrystalline and aperiodic structures, *Physica E: Low-Dimensional Syst. Nanostruct.* **42**, 1871 (2010).